

Improved Pt/C electrocatalysts for methanol oxidation prepared by different reducing agents and surfactants and DFT studies on it

Aysu Çokangın · Metin Aydın · Gülsün Göktaş

Received: 5 July 2017 / Accepted: 2 October 2017 / Published online: 14 October 2017
© Springer Science+Business Media B.V. 2017

Abstract In this work, PtCl₄ as precursor; sodium borohydride (Cat I), hydrazinium hydroxide (Cat II), and formaldehyde (Cat III) as reducing agents; and 1-heptanamine (a), N-methyl-1-heptanamine (b), and N,N-dimethyl-1-heptanamine (c) as surfactants were used to prepare platinum nanoparticles which were then dispersed on carbon XC-72 for use as catalysts in the methanol oxidation reaction. XRD and TEM results indicate that the platinum has a face-centered cubic structure and is found as small and agglomerated particles in different shapes, sizes, and densities. Cat I comprises small (~5 nm) cubic and formless agglomerated (~20~300 nm) particles, Cat II is composed of small (~5 nm) and a significant number of quite dense spherical agglomerated (~20~150 nm) particles, and Cat III contains large number of small (~5 nm) and a small number of spherical, less dense, and agglomerated (~20~200 nm) particles. XPS data shows that the platinum exists in two different oxidation states Pt(0) (~64.5~69.6%) and Pt(IV) (~35.5~30.4%), and platinum surface also contains OH, H₂O, C–O, C=O, and

carbon. DFT and FTIR show that the surfactants decompose to form partially crystalline carbon. Electrochemical studies reveal that performance order of the catalysts towards the methanol oxidation reaction is Cat II < Cat I < Cat III, and that Cat IIIc has the highest performance, which is 2.23 times larger than E-TEK catalysts. It was found that the performance of the catalysts depends on the kind of surfactant, reducing agent, electrochemical surface area, percent platinum utility, roughness factor, and I_p/I_r ratio.

Keywords Methanol oxidation · Carbon support · Platinum nanoparticles · Catalyst performance · X-ray photoelectron spectroscopy

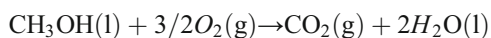
Introduction

The increasing demand for energy and deficiency of conventional energy sources has lead researchers to discover alternative methods of power generation (Asif and Muneer 2007). One of the important developments in electrochemistry is the conversion of chemical energy into electrical energy via fuel cells (Hordeski 2009; Bagotsky 2012; Carette et al. 2000). Fuel cells are a developing technology as a means of clean energy production that are popular with researchers. It is believed that they will play an important role in the energy industry in the future (Hordeski 2009). Direct methanol fuel cells, DMFCs, are one type of fuel cell where methanol is oxidized at the anode and oxygen is reduced

A. Çokangın · G. Göktaş (✉)
Chemistry Department, Middle East Technical University,
06800 Ankara, Turkey
e-mail: ggulsun@metu.edu.tr

M. Aydın
Department of Chemistry, Faculty of Art and Sciences, Ondokuz
Mayis University, 55139 Samsun, Turkey

at cathode and the overall reaction is (Bagotsky 2012; Carrette et al. 2000; Li 2006; Zeng et al. 2006):



DMFCs have many advantages such as being environmentally friendly, having high energy density, no storage problems, and low operating temperature (Zeng et al. 2006; Wang et al. 2003; Hogarth and Hards 1996; Hart and Womack 1967, Wasmus and Küver 1999). The main limitation of DMFCs is that methanol is electrochemically inactive, therefore a catalyst is needed. Catalysts include metal nanoparticles on a support such as carbon, carbon nanotubes and conductive polymers (Li 2006; Hart and Womack 1967; Wasmus and Küver 1999; Arico et al. 2001; Kulkarni et al. 2012; Ahmed et al. 2013; Şen et al. 2013). Platinum nanoparticles are promising catalysts and different kinds of methods have been employed in their preparation, mainly chemical and electrochemical. One chemical preparation method utilizes a surfactant (stabilizer) and reducing agent (Arico et al. 2001; Zheng 2012; Carrette et al. 2001; Kulkarni et al. 2012; Stambouli and Traversa 2002; Singh and Datta 2010; Ahmed et al. 2013; Şen et al. 2013; Şen and Gökağaç 2014). Researches have shown that the kind of surfactant and reducing agent have significant influence on the shape, size, and morphology of the platinum nanoparticles. In order to explore the reasons behind for this, different surfactant and reducing agents were used in this study to prepare platinum nanoparticles. The particles were then dispersed on carbon XC-72 to prepare new catalysts for the methanol oxidation reaction used in direct methanol fuel cells. These catalysts were characterized using XRD, XPS, TEM, ICP, and their electrochemical properties and performance were defined by cyclic voltammetry. In addition to this, DFT analysis were done to compute IR spectra of isolated, dimer, and adsorbed 1-heptanamine on platinum and to determine the binding energies between platinum, (111), (110), and (100) planes, and adsorbed species, CO_{ads} , OH_{ads} , and $\text{H}_2\text{O}_{\text{ads}}$.

Experimental methods

Materials

PtCl_4 (99%, Alfa), NaBH_4 (96%, Merck), $\text{N}_2\text{H}_5\text{OH}$ (100%, Merck), formaldehyde (37%, Merck), N,N-

dimethylformamide (99.8%, Merck), 1-heptanamine (99%, Sigma-Aldrich), N-methyl-1-heptanamine (96%, Sigma-Aldrich), N,N-dimethyl-1-heptanamine (98%, Sigma-Aldrich), NaOH (99%, Merck), toluene (99%, Merck), $\text{C}_2\text{H}_5\text{OH}$ (99.2%, Merck), CH_3OH (99.8%, Merck), CCl_4 (99%, Merck), HClO_4 (60%, Merck), nafion (5%, Sigma-Aldrich), and Vulcan carbon XC-72 (Cabot Europa Ltd.) were used as received. A Millipore water purification system was utilized to produce deionized water (18 M Ω).

The synthesis of Cat Ia

0.0808 g (0.24 mmol) of PtCl_4 was dissolved in 120 mL deionized water and stirred for 20 min. Then, 0.22 mmol of freshly prepared NaBH_4 solution was added dropwise to achieve the reduction of Pt^{+4} to Pt^0 . A change in color from yellow to black and the end of hydrogen gas evolution was observed before proceeding. Two phases were formed upon addition of 0.24 mmol of 1-heptanamine surfactant in 120 ml of toluene and platinum particles were observed in the intermediate phase. 1.4 mL of 1 M NaOH solution was then added into the black solution to achieve better phase separation and the mixture was stirred for 2 hr to complete the reaction. All these processes were performed under a high purity argon atmosphere. The solution was then centrifuged for 30 min, the washing process was performed seven times with dry ethanol to remove impurities. Finally, the product was dried under vacuum at room temperature.

Synthesis of Cat IIa

0.0808 g (0.24 mmol) of PtCl_4 was added to 120 mL deionized water and dissolution was completed by stirring for 20 min. Then, 2.4 mmol of $\text{N}_2\text{H}_5\text{OH}$ solution was added to the solution dropwise to reduce Pt^{+4} to Pt^0 . During this process, the color changed from yellow to grayish black. Afterwards, 120 mL of toluene with 0.24 mmol of 1-heptanamine was introduced into the solution. The rest of the synthetic procedure was the same as for Cat Ia.

Synthesis of Cat IIIa

0.24 mmol of PtCl_4 complex was dissolved in 120 mL of deionized water. The solution was heated up gradually to 70 °C and the pH of the solution was adjusted to 9–10 by adding 2.5 M NaOH solution to provide better

reduction medium. For the reduction process, 0.48 mmol of formaldehyde was added to this solution and mixing was continued until the observation of a grayish black solution. Afterwards, 120 mL of toluene solution with 0.24 mmol of 1-heptanamine surfactant was added to this mixture. All these processes were carried out under the high purity argon atmosphere. The rest of the synthetic procedure was the same as for Cat Ia and IIa.

Synthesis of Cat Ib, IIb, IIIb, Ic, IIc, and IIIc

The same synthetic methods were followed to prepare Cat b and c catalysts, the reducing agents were the same but the surfactants were different (N-methyl-1-heptanamine and N,N-dimethyl-1-heptanamine). The catalyst ID, surfactant and the reducing agents used are listed in Table 1.

Electrode preparation

0.5 mL of nafion, 0.15 mL of N, N-dimethyl formamide, and 2.5 mL of distilled water was added to 36.78 mg carbon-supported powder catalyst which contains one portion of mostly platinum containing sample and ten portions of carbon XC-72. The resulting mixture was ultrasonicated for a few days to obtain a homogeneous slurry solution. Fifty microliter of this solution was dropped on a glassy carbon with a diameter of 0.7 cm. Then dried at 40 °C for 20 min, 65 °C for 20 min, and finally 100 °C for 1 h to provide good “adhesion” of the catalyst on the surface of the glassy carbon electrode (Şen et al. 2011) This was used as a working electrode for electrochemical measurements.

Table 1 Catalyst ID, surfactants and reducing agents used in their synthesis

Catalysts	Reducing agents	Surfactants
Cat Ia	Sodium borohydride	1-heptanamine
Cat Ib		N-methyl-1-heptanamine
Cat Ic		N,N-dimethyl-1-heptanamine
Cat IIa	Hydrazinium	1-heptanamine
Cat IIb	hydroxide	N-methyl-1-heptanamine
Cat IIc		N,N-dimethyl-1-heptanamine
Cat IIIa	Formaldehyde	1-heptanamine
Cat IIIb		N-methyl-1-heptanamine
Cat IIIc		N,N-dimethyl-1-heptanamine

Characterization techniques

Inductively coupled plasma spectroscopy

Perkin Elmer Optima 4300DV was used for ICP measurements using the following settings: ICP RF power 1300 W, plasma gas flow 15 L.min⁻¹, nebulizer gas flow 0.8 L.min⁻¹, auxiliary gas flow 0.2 L.min⁻¹, and sample uptake rate 1.5 ml.min⁻¹ replicates 3. The results given in Table 2 were used to plot the cyclic voltammograms in A/mg Pt.

X-ray diffraction

Rigaku Miniflex diffractometer with Ultima + theta-theta high resolution goniometer operating at 30 kV, 15 mA, was utilized for XRD diffraction measurements.

Transmission electron microscopy

JEOL 200 kV TEM was employed for TEM images. The electron microscopy samples were prepared by ultrasonating catalysts in CCl₄ until a homogeneous mixture was obtained, then the suspended mixture was dropped on the carbon covered copper grid with a 400 mesh and dried at room temperature.

Brunauer–Emmett–Teller

Autosorb 6B instrument (Quantachrome Co.) was applied to define surface area of samples. Samples were gassed out at 30 °C for 16 h to remove residual water and gases before measurements, and nitrogen was used as an adsorbent. The multipoint method at relative pressure of P/P₀ = 0.05 up to P/P₀ = 0.3 at 77.4 K was the experimental conditions employed.

X-ray photoelectron spectroscopy

SPECS spectrometer with X-ray source of Mg K_α lines operating at 1253.6 eV, 10 mA, was utilized to report XPS spectra of samples which do not contain carbon XC-72 support. The C 1s line at 284.6 eV was taken as reference point and the peak fitting was performed using Lorentzian- Gaussian method.

Table 2 Average particle size of small platinum particles estimated from (A) XRD and (B) TEM (agglomerated particles were not considered), % Pt (ICP results), and average surface area (BET results)

Catalysts	A	B	% Platinum	Average surface area (BET results)
Cat Ia	~5.3 nm	~4.9 ± 1.0 nm	93.4 ± 1.0	29.24 m ² /g
Cat Ib	~5.5 nm	~5.1 ± 0.8 nm	88.3 ± 1.1	
Cat Ic	~5.2 nm	~4.9 ± 0.9 nm	92.5 ± 0.4	
Cat IIa	~4.1 nm	~4.0 ± 0.7 nm	88.5 ± 0.6	6.00 m ² /g
Cat IIb	~4.9 nm	~4.6 ± 0.6 nm	87.3 ± 1.0	
Cat IIc	~4.5 nm	~4.6 ± 0.8 nm	89.2 ± 0.6	
Cat IIIa	~5.2 nm	~4.8 ± 0.7 nm	92.3 ± 0.5	38.73 m ² /g
Cat IIIb	~4.1 nm	~4.3 ± 0.8 nm	92.0 ± 0.7	
Cat IIIc	~4.9 nm	~4.9 ± 0.7 nm	93.8 ± 0.5	

Fourier transfer infrared

FTIR spectra were gathered using a Bruker 66 v/s using KBr pellets with 15 scans at room temperature.

Cyclic voltammetry

A computer-controlled potentiostat/galvanostat, Solartron 1285 was employed to determine the electrochemical properties and electrocatalytic performance of catalysts towards the methanol oxidation reaction. Glassy carbon, saturated calomel electrode, and the prepared catalysts fixed on a glassy carbon were used as counter, reference, and working electrodes, respectively.

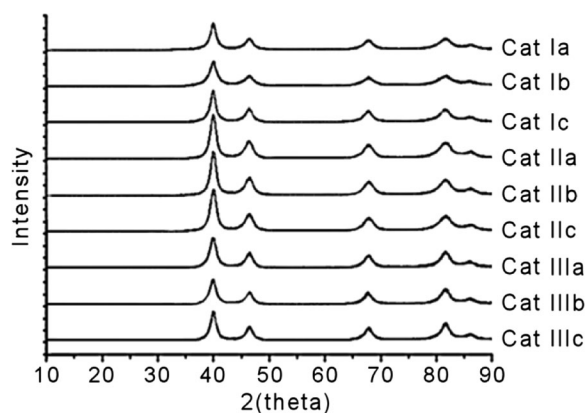
Density functional theory

The IR spectra of the isolated, dimer, and adsorbed 1-hexanamine on platinum nanoparticles were calculated using the density functional theory (DFT) at the CAM-B3LYP/Lan12DZ level and the binding energies between different sides of platinum (Pt(111), Pt(110), and Pt(100)) and adsorbed species (CO_{ads}, OH_{ads}, and H₂O_{ads}) were determined by B3LYP/Lan12DZ level.

Results and discussion

X-ray diffraction patterns of all catalysts are given in Fig. 1. As can be seen from the figure, the characteristic features of face-centered cubic (fcc) structure of

platinum were observed at 39.9, 46.35, 67.75, and 81.25° which correspond to the (111), (200), (220), and (311) planes of platinum, respectively (JCPDS cards 04-0802). Utilizing XRD data, an average crystallite size of platinum was also obtained using the Scherrer formula: $d(\text{Å}) = k\lambda/(\beta\cos\phi)$, where d = average particle size, k = Scherrer constant (0.9), λ = wavelength of the incident x-ray (1.54056 Å), β = full width half-maximum of XRD peak in rad, and ϕ = the angle that correspond to the peak position at maximum height (Chatterjee 2010). The average crystallite size of platinum in all catalysts was found to be ~5 nm (Table 2); there is very little difference in size between the catalysts. However, it should be kept in mind that XRD only can indicate average crystallite size. Therefore, these results should be confirmed by transmission electron microscopy (TEM).

**Fig. 1** XRD patterns of the catalysts

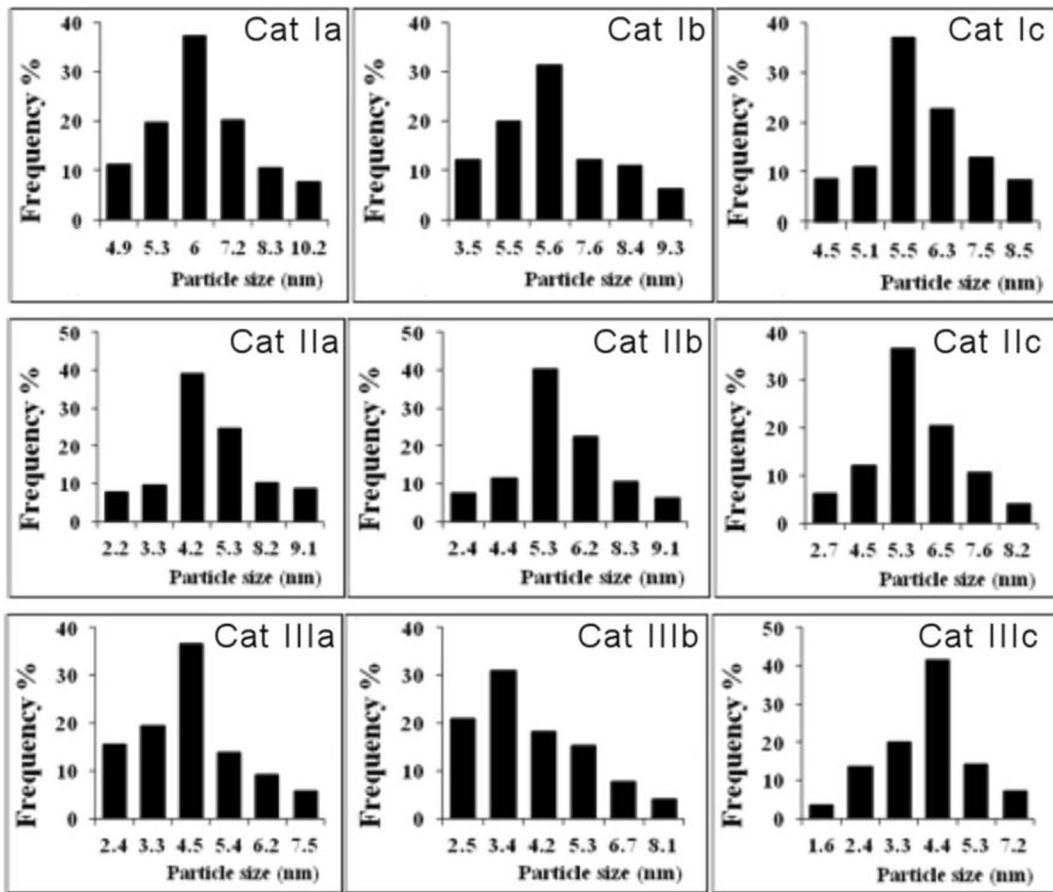
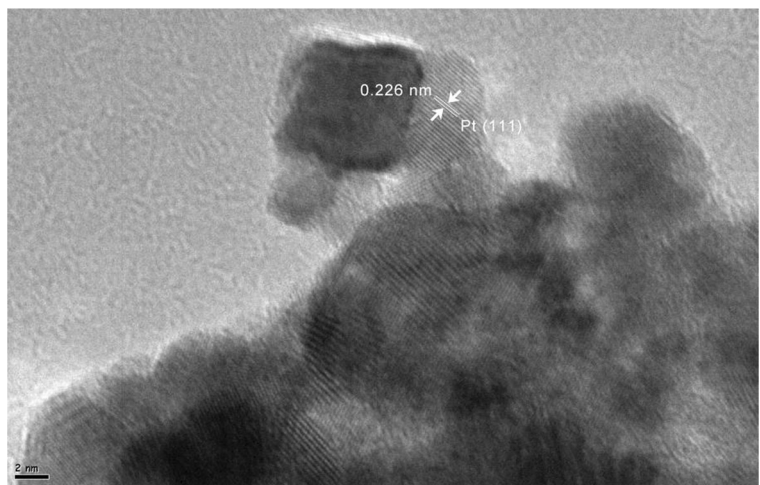


Fig. 2 The size distribution histograms of platinum nanoparticles in all catalysts, agglomerated particles are not included

Average and individual sizes of the platinum particles and their distribution on carbon support were determined by TEM. The average particle size of the platinum particles was calculated by considering about 500

particles from different regions of all catalysts and size distribution histograms are plotted in Fig. 2. The average platinum particle size was found to be ~5.0 nm which is consistent with XRD data. TEM also shows that Cat II

Fig. 3 HR-TEM image of Cat Ia



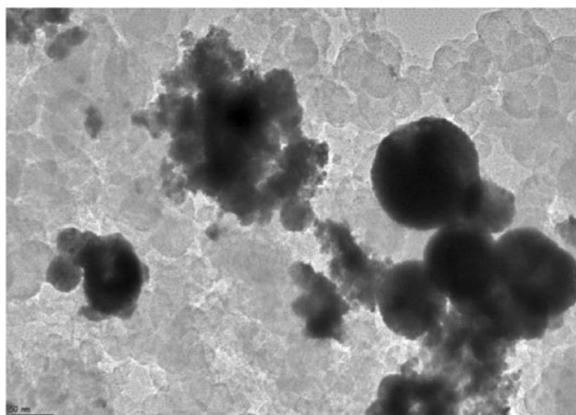


Fig. 4 TEM image of Cat IIb

and III consist of spherical platinum nanoparticles, while Cat I has a cubic form (Fig. 3). Figure 3 also shows atomic lattice fringes of Pt(111) with spacing of 0.226 nm, which is close to the standard Pt(111) spacing of 0.228 nm (Liang et al. 2005). Similar cubic forms were reported by Yang et al. who used NaBH_4 as a reducing agent (Yang et al. 2004a, Yang et al. 2004b). Besides the shape of individual particles, the number of small particles between each group (Cat I, II, and III) was also estimated from TEM images, and it was observed that Cat III has the largest number of small particles while Cat II has the least. To confirm these results, BET analyses were carried out for all catalysts which do not contain carbon XC-72 and it was found that Cat III has the highest average surface area ($38.73 \text{ m}^2/\text{g}$ sample), while Cat II has the smallest ($6.00 \text{ m}^2/\text{g}$ sample), Table 2, which is in good agreement with the TEM data. In addition to these small platinum particles, agglomerated particles composed of small nanoparticles were also observed for all catalysts. The

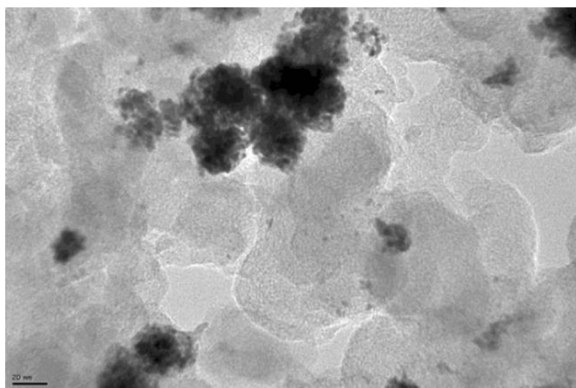


Fig. 5 TEM image of Cat IIIb

number and morphology of the large particles changes from one group to another, for instance the shape of large particles in Cat Ia–c were not in perfectly spherical in form, but it is still possible to estimate the approximate size of these large particles (between 20 and 150 nm). On the other hand, most of the particles were large, spherical, and compact in Cat II with a size of 20–300 nm (Fig. 4), and similar spherical and agglomerated particles (20–200 nm) were observed for Cat III (Fig. 5) but they are not as dense as in Cat II.

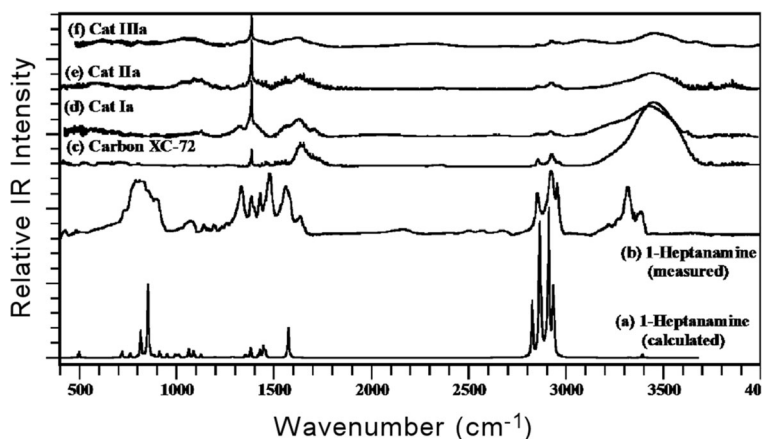
In summary:

- Cat I contains mostly small (~ 5 nm) cubic and formless agglomerated (~ 20 – 150 nm) platinum nanoparticles,
- Cat II consists of predominantly spherical, dense, and large (~ 20 – 300 nm) platinum nanoparticles, in addition to a few small nanoparticles (~ 5 nm), and
- Cat III consists of small platinum nanoparticles (~ 5 nm), besides large (~ 20 – 200 nm), and less dense platinum particles, compared to Cat II.

Inductively coupled plasma spectroscopy results indicated that the platinum content of each sample, which does not include any carbon support, was about 90% platinum and about 10% of other material such as surfactant (Table 2). In order to confirm this, FTIR spectra of all surfactants, samples, and carbon XC-72 were obtained in the range of 400 – 4000 cm^{-1} . All surfactants indicated the characteristic FTIR peaks and as an example only 1-heptanamine is shown in Fig. 6. This figure also shows 1-heptanamine in water (calculated), carbon XC-72, Cat Ia, IIa, and IIIa. To assign each observed peak, the IR spectrum of 1-heptanamine was carried out in water (used as a solvent) at CAM-B3LYP^{M1} level of the DFT theory using 6311++G(d,p) basis set. Here, the solvent effects were considered using the self-consistent reaction field (SCRF) calculations (Tomasi et al. 2005) with the conductor-like polarizable continuum model (CPCM) (Barone and Cossi 1998) with a dielectric constant of 78.39 for water, SCRF=(CPCM, Solvent=Water) as contained in the Gaussian 09 software package (Frisch et al. 2009, Gaussian 09 Revision). The nuclear motion of the atoms within molecule using the Gaussview *visualization* program was used to assign each IR peak in their spectrum. The results of the calculations can be summarized as follows: (a) the observed IR peak at 490 cm^{-1} (calculated peak at 497 cm^{-1}) is due to bending deformation of C–C–N

Fig. 6 FTIR spectra of 1-heptanamine in water (calculated) (a), 1-heptanamine (observed) (b), carbon XC-72 (c), Cat Ia (d), Cat IIa, (e), and Cat IIIa (f). It is worth noting that the calculated vibrational frequencies coincide with those observed in the IR spectrum of the 1-heptanamine using a scaling factor:

$$\nu_{ca} = 30.5 + (0.935)\nu_{ca}$$



bond; (b) the observed IR features at 730, 820, 879, 1071, and 1139 cm^{-1} are assigned to predicted IR peaks at 719, 814, 880, 1086, and 1124 cm^{-1} , which result from rocking, wagging, and twisting of the CH_2 , CH_3 , and NH_2 groups and bending deformation of the C-C-C bonds; (c) the calculated peaks at 1353, 1379, 1426, 1455, and 1572 cm^{-1} are mainly due to the intramolecular bending deformation, which are observed at 1339, 1383, 1430, and 1473 cm^{-1} in the IR spectrum; (d) the symmetric and asymmetric stretching modes of CH_2 and CH_3 were predicted in the range of 2826–2873 cm^{-1} and 2911–2937 cm^{-1} , respectively, which correspond to observed ones at about 2850 (symmetric stretching), 2919 and 2951 cm^{-1} (asymmetric stretching); and (e) while the measured FTIR spectra of the 1-heptanamine molecule was produced two peaks at about 3391 and 3313 cm^{-1} , its experimental spectrum in gas phase and calculated IR spectra in water (used as solvent) did not show any active IR peaks due to NH_2 bond stretching. When intermolecular hydrogen bonding interaction, however, was considered between neighbor molecules ($\text{C}_7\text{H}_{17}\text{N}$ - - $\text{HNH}_{16}\text{C}_7$) and calculated at the CAM-B3LYP/6-311++G(d,p) level, two IR peaks as a result of the symmetric and asymmetric NH_2 stretching at 3325 and 3393 cm^{-1} , respectively, were predicted in Fig. 6b. The full assignment of the FTIR spectrum is given in Table 3. As seen in Fig. 6a, the observed and calculated IR spectra of 1-heptanamine are quite different from Cat a. As a result, it is believed that 1-heptanamine was decomposes during the synthetic procedure. This result also is verified by the calculated IR spectra of 1-heptanamine adsorbed on the Pt(111). If 1-heptanamine were attached on the platinum, IR peaks would have been seen above 3278 and 3363 cm^{-1}

(resulting from the NH bond stretching), and a new and enhanced peak at 1090 and 1599 cm^{-1} , respectively. In addition to this, the red and blue shifts in the IR band positions relative to the isolated 1-heptanamine was also expected as shown in Fig. 7 and Table 3. A new peak, red, and blue shifts were not observed in the measured spectra of Cat a; on the other hand, its spectra shows similarities to the carbon XC-72 spectrum, indicating that 1-heptanamine decomposes to form partially crystalline carbon.

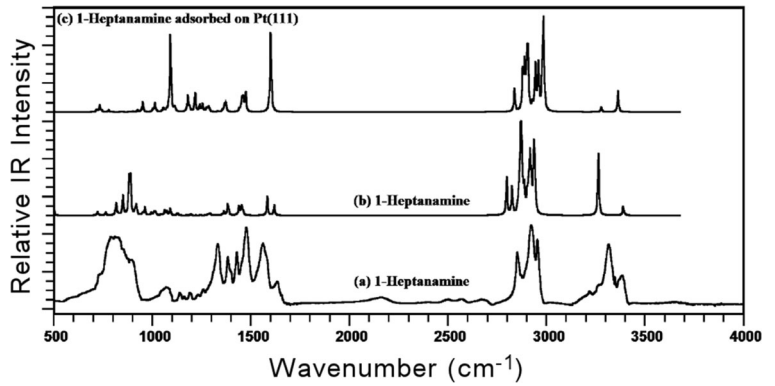
X-ray photoelectron spectroscopy, XPS, was employed to investigate the oxidation states and relative amount of elements for a given sample (no carbon support). For this purpose, Pt 4f, O 1s, and C 1s regions of the XPS spectra for all catalysts were recorded and the Gaussian-Lorentzian method was used to analyze these peaks. The Pt 4f peak was evaluated by keeping a 3.35 eV difference and 3:4 intensity ratio between $4f_{5/2}$ and $4f_{7/2}$ doublets as much as possible, Fig. 8a–i, and the results are given in Table 4. The peak fitting analyses indicate that the Pt 4f peak of all catalysts consist of two doublets, one at ~ 71.1 eV ($4f_{7/2}$) and ~ 74.4 eV ($4f_{5/2}$), and the other one at ~ 74.4 eV ($4f_{7/2}$) and ~ 77.7 eV ($4f_{5/2}$) (Şen et al. 2011; Şen and Gökağaç 2007; Gökağaç et al. 1993). The first doublet belongs to Pt(0) and the second one is associated with a Pt(IV) species, such as PtO_2 and/or $\text{PtO}(\text{OH})_2$ and/or $\text{Pt}(\text{OH})_4$. Binding energy (BE) comparison within each group demonstrated that the three Cat a (Ia, IIa, and IIIa) have lower values compare to the others which might be due to lower electron donation from platinum to the environmental elements for Cat a compared to Cat b and c. The Pt (0)/Pt (IV) relative ratio was also calculated by using the peak area under each doublet and was found

Table 3 Active IR frequencies (in cm^{-1}) of 1-heptanamine: (a) observed (on KBr in the first column), (b) calculated in water used as solvent in second column, (c) dimerized 1-heptanamine molecule (in gas phase, in third column), (d) and 1-heptanamine adsorbed on Pt(111) surface. The calculations have been done at CAM-B3LYP/6-311++G(d,p) level of density functional theory.

The solvent effect was taken into consideration by using the self-consistent reaction field (scrf=(cpcm, solvent=water) as contained in the Gaussian 09 software package)). The calculated IR spectra were fitted to observed spectrum by using a scaling factor, $\nu_{\text{sc}} = 30 + 0.395 \times \nu_{\text{ca}}$

(a)		(b)		(c)		(d)		Assignment
ν_{ob}	I_{IR}	ν_{sc}	I_{IR}	ν_{sc}	I_{IR}	ν_{sc}	I_{IR}	
490	5	497	4	498	7	490	1	Bending deformation of C–C–N bond
730	30	719	4	720	3	731	9	Rocking of the CH_2 and CH_3 , accompanied by wagging of NH_2
820	85	760	3	762	4	742	2	Rocking and twisting CH_2 and CH_3 , including wagging of NH_2
		814	19	814	12	776	2	
859	70	851	54	849	31	842	1	Primarily due to the wagging of NH_2 , including twisting of the CH_2 and CH_3
879	56	880	1	883	1	900	1	Rocking of CH_3 and relatively weak symmetric stretching of $\text{C}(\text{H}_3)\text{--C--C}$ bonds
				880	53			Rocking of CH_3 , wagging of NH_2 and relatively weak symmetric stretching of $\text{C}(\text{H}_3)\text{--C--C}$ bonds
				887	56			
902	56	911	4	910	6	923	2	Wagging of NH_2 and twisting of CH_2
				917	16			
		950	3	947	3	949	12	Symmetric stretching of C–C–N and C–C–C bonds, including twisting of NH_2 and CH_2
				960	13			
		991	2	992	2	1000	3	Twisting of CH_2 and NH_2 groups
				994	3			
1071	22	1060	6	1061	8	1011	10	Mainly due to the asymmetric stretching of C–C–N bond
				1072	6	1054	4	
						1090	93	Primarily due to the NH_2 wagging and relatively weak twisting of $\text{C}(1)\text{H}_2$ and $\text{C}(2)\text{H}_2$ groups
		1086	5	1089	6	1113	5	Primarily due to rocking of the CH_3 and NH_2 groups, accompanied by C–C bond stretching and bending deformation within the molecule
				1090	5			
1139	15	1124	2	1123	2			Primarily due to bending deformation within the molecule, accompanied by rocking of the CH_3 and twisting of CH_2 and NH_2 groups
				1129	3			
1193	15	1194	1	1194	1	1178	19	Wagging of the CH_2 and CH_3 , including twisting of NH_2
				1195	<1	1216	23	
1318	50	1279	1	1280	1	1253	10	Twisting of CH_2 and NH_2 groups
	sh	1288	1	1286	2	1285	6	
				1293	3			
1332	76	1353	2	1361	3	1371	10	Out of plane bending deformation of the CH_3 like open-close umbrella shape and relatively weak $\text{C}(\text{H}_3)\text{--C}(\text{H}_2)$ bending stretching
1383	60	1379	7	1381	16	1381	1	Primarily due to C–C(N) bond stretching and wagging of their H atoms
				1386	7			
1430	66	1426	5	1438	6	1454	7	Due to bending deformation within the CH_3 group
				1438	6			
1454	53(sh)	1445	8	1452	8	1460	13	Scissoring (in-plane bending deformation) of CH_2 groups
1473	96	1455	4	1458	4	1472	22	
1565	77	1572	22	1582	31	1599	100	NH_2 scissoring
1634	29			1617	16			NH_2 scissoring
2850	65	2826	40	2797	60	2837	27	Symmetric stretching of CH bonds
		2863	47	2824	44	2879	31	
		2866	70	2869	59	2880	11	
		2873	15	2870	58	2888	51	
		64	3073	2887	37	2903	35	
2919	100	2911	100	2916	83	2943	56	Asymmetric stretching of CH bonds
2951	81	2931	41	2923	42	2958	55	
		2937	25	2936	38	2984	99	
3316	76	3325	<1	3263	100	3278	6	Symmetric NH_2 bond stretching
3386	37	3393	2	3389	14	3363	25	Asymmetric NH_2 bond stretching

Fig. 7 1-Heptanamine measured (a), 1-heptanamine (dimer) calculated (b), 1-heptanamine adsorbed on Pt(111) (c).



that the ratio changes between 64.5/35.5 and 69.6/30.4. It was noted that the three Cat b (Ib, IIb, and IIIb) have the smallest Pt (0) to Pt (IV) ratio, while the three Cat c (Ic, IIc, and IIIc) have the largest one; once again when

comparison is done within each group. These results revealed that the kind of surfactant affects the peak position and oxidation state ratio of platinum. An O 1s region analyses were accomplished by keeping the peak

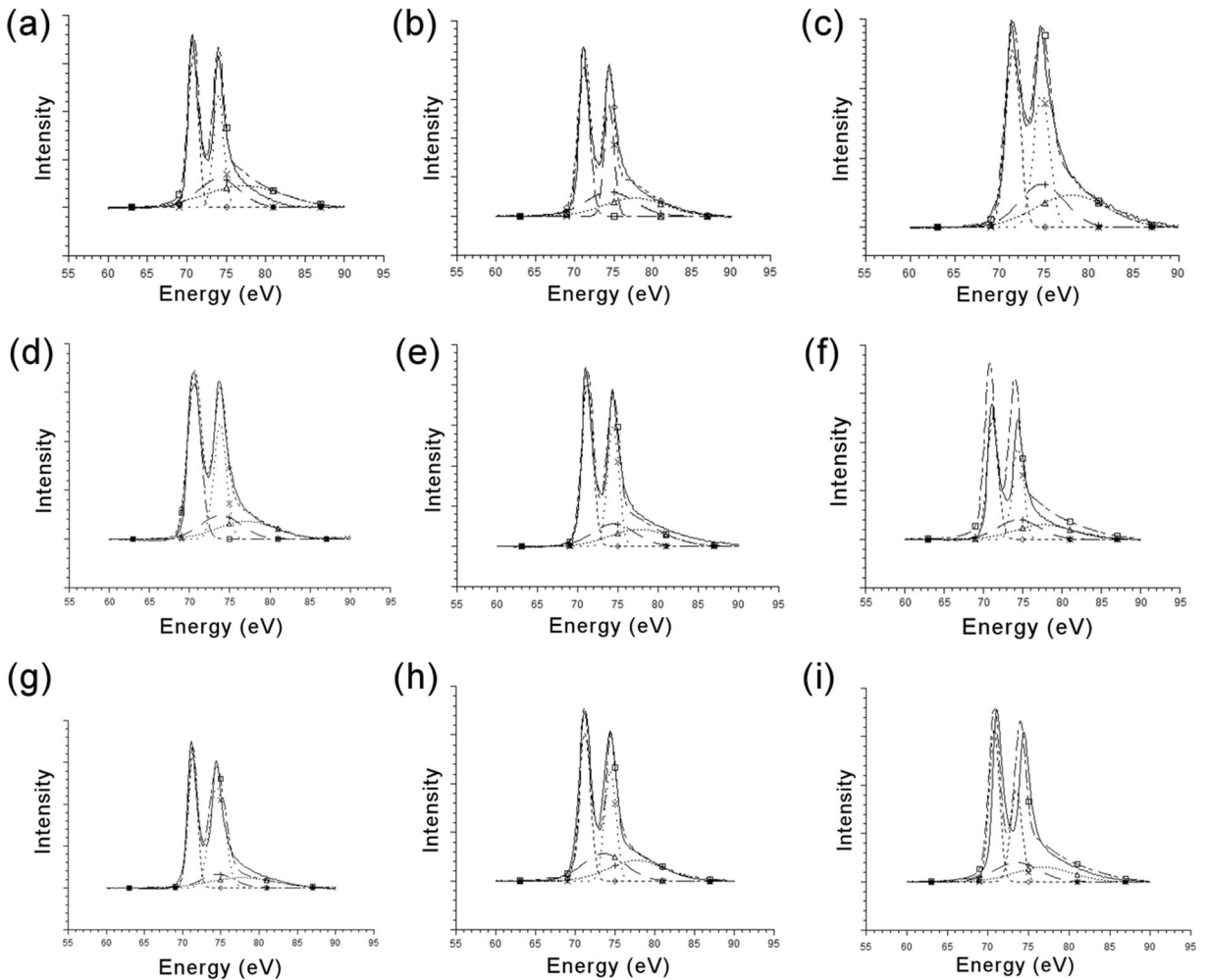


Fig. 8 Pt 4f electron spectra of Cat a Ia, b Ib, c Ic, d IIa, e IIb, f IIc, g IIIa, h IIIb, and i IIIc

Table 4 Pt 4f7/2 core binding energies, eV, in the prepared catalysts which do not contain carbon support and the relative intensities of the species

Catalysts	Pt 4f _{7/2}	Pt 4f _{7/2}	Pt(0)/Pt(IV)	O 1s	O 1s	O 1s	C 1s	C 1s	C 1s
	Pt(0)	Pt(IV)	Pt(0)/Pt(IV)	OH _{ads} and/or CO _{ads}	(H ₂ O _{ads})	C=C (sp ²)	C-C (sp ³) and/or COH and/or CO	(C=O)	
Cat Ia	70.8 (67.7)	74.0 (32.3)	2.09	531.0 (83.4)	532.0 (16.6)	284.0 (74.2)	285.0 (6.5)	287.8 (19.3)	
Cat Ib	71.2 (64.5)	74.4 (35.5)	1.82	531.5 (85.5)	532.5 (14.5)	284.1 (67.2)	285.3 (11.8)	287.7 (21.0)	
Cat Ic	71.4 (69.6)	74.6 (30.4)	2.29	531.8 (83.9)	532.8 (16.1)	284.1 (74.6)	285.5 (6.8)	287.5 (18.6)	
Cat IIa	70.6 (67.4)	73.8 (32.6)	2.07	531.3 (88.6)	532.0 (11.4)	284.0 (73.4)	285.4 (5.2)	287.4 (25.4)	
Cat IIb	71.2 (66.4)	74.4 (33.6)	1.98	531.3 (90.0)	532.0 (10.0)	284.2 (69.2)	285.6 (8.8)	287.6 (22.0)	
Cat IIc	71.2 (69.0)	74.4 (31.0)	2.22	531.3 (89.2)	532.0 (10.8)	284.2 (69.4)	285.7 (8.2)	287.3 (22.4)	
Cat IIIa	70.8 (67.2)	74.1 (32.8)	2.05	531.9 (80.1)	532.8 (19.9)	284.3 (69.3)	285.0 (8.7)	287.3 (22.0)	
Cat IIIb	71.2 (65.3)	74.4 (34.7)	1.88	531.8 (77.4)	532.6 (22.6)	284.5 (65.0)	285.4 (8.3)	287.4 (26.7)	
Cat IIIc	71.3 (69.4)	74.5 (30.6)	2.27	531.2 (78.9)	532.3 (21.1)	284.5 (64.5)	285.0 (8.4)	287.6(27.1)	

half width of ~ 1.6 eV, and indicates that O 1s peak consists of two peaks for all catalysts, one at 531.0–531.9 eV and the other one at 532.0–532.8 eV, Table 4. Former studies indicates that the first peak could be due to adsorbed OH (HO_{ads}) (Xia 2013) and/or most probably adsorbed CO (CO_{ads}) (Wu et al. 2014; Kvande et al. 2010), while the second peak could be due to adsorbed H₂O (H₂O_{ads}) (Casella et al. 1999; Luo et al. 1996) on the surface of catalysts. The amount of H₂O_{ads} is ~ 15 , ~ 10 , and $\sim 20\%$ for Cat I, II, and III, respectively. It is believed that the amount of H₂O_{ads} is most probably influenced by reducing agent, but not surfactant, because there is no obvious relationship between the kind of surfactant and H₂O_{ads}. Besides the Pt 4f and O 1s regions, the C 1s region of XPS for all catalysts was also evaluated and the results were reported in Table 4. As mentioned previously, the XPS measurements were done before addition of carbon support to the platinum containing sample. Therefore, C 1s peak does not come from support material, but residue which could not be removed during washing process. Detailed information about the residue will be presented later in the DFT section. In general, the C 1s region consists of three peaks at ~ 284.2 , ~ 285.3 , and ~ 287.5 eV corresponding to sp² carbon atoms (C=C) in partially crystalline carbon (Yang et al. 2011); C in C–C (sp³) (Huang et al. 2012) and/or C in C–OH (Rao et al. 2014; Tien et al. 2012) and/or most probably C–O (Huang et al. 2014); and C in carbonyl (C=O) (Huang et al. 2012; Senthilnathan et al. 2014), respectively.

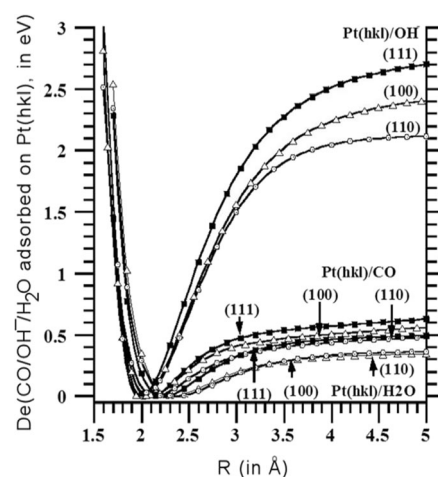
**Fig. 9** The calculated binding energies of adsorbed of OH⁻, CO and H₂O molecules on the (111, black square), (110, white triangle), and (100, white circle) surfaces of the platinum

Table 5 Potential energy surface (PES) scan of the adsorption of OH⁻, CO, and H₂O molecules on the (111, black square), (110, white triangle), and (100, white circle) surfaces of the Pt

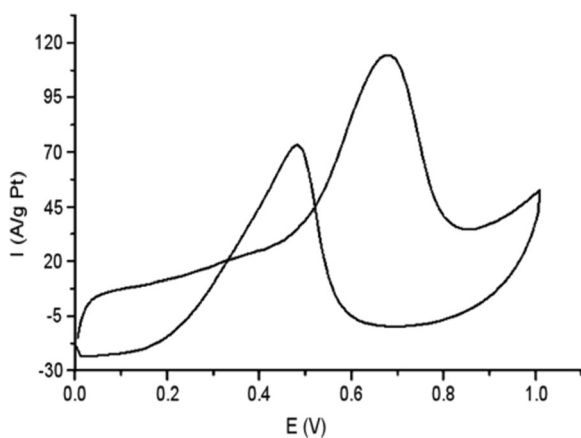
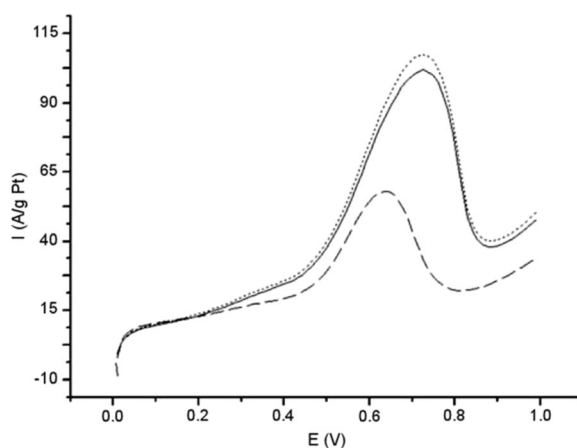
	OH ⁻			CO			H ₂ O		
	(eV)	R _e (Å)	R _d (Å)	(eV)	R _e (Å)	R _d (Å)	(eV)	R _e (Å)	R _d (Å)
Pt(111)	2.711	2.00	5.15	0.672	2.30	6.05	0.520	2.30	6.20
Pt(100)	2.414	1.95	5.10	0.594	2.05	5.80	0.367	2.30	6.20
Pt(110)	2.113	2.00	5.00	0.500	2.20	5.80	0.377	2.30	6.20

Estimation of the bond strength between the platinum and adsorbed species such as CO_{ads}, OH⁻_{ads}, and H₂O_{ads} was done by using the B3LYP/LanL2DZ level of the theory. For that reason, the binding energies between Pt(111), Pt(110), and Pt(100) planes, and CO_{ads}, OH⁻_{ads}, and H₂O_{ads} were computed and found that the strongest and weakest bonds are formed between platinum and OH⁻ and H₂O, respectively (Fig. 9 and Table 5). It was also noticed that the highest binding energies were obtained between Pt(111) and the adsorbed species.

The electrochemical properties and performance of the prepared catalysts towards the methanol oxidation reaction were determined by cyclic voltammetry. Cyclic voltammograms of catalysts were similar and all exhibited typical hydrogen and oxygen adsorption/desorption regions in 0.1 M HClO₄ solution at room temperature. In case of methanol addition to the HClO₄ electrolyte, a great change is seen (Fig. 10). Essentially, the methanol electro oxidation

nanoparticles. Re and Rd indicate distances between molecule and Pt-surface at the equilibrium distance and at the non-interaction distance (or dissociation limit), respectively

reaction starts at ~0.40 V and reaches maxima at 0.7 V in the forward scan and incompletely oxidized intermediate species such as CO starts to be removed from the catalyst surface at ~0.55 V and maximum current was observed at 0.45 V in the reverse scan. In order to observe the performance difference between the catalysts more easily, only the anodic part of the cyclic voltammograms were considered and are shown in Figs. 11, 12, 13, 14, 15, and 16. Cyclic voltammograms were recorded with the aim of exploring two parameters, (a) surfactant type and (b) reducing agent used for catalysts preparation. When the type of surfactant was kept constant and reducing agents was changed (Figs. 11, 12, and 13), the same trend was observed for all groups and it was found that the most active catalyst was Cat III which was prepared with formaldehyde and the least active one was Cat II which was synthesized using hydrazinium hydroxide. When the type of reducing agent was kept

**Fig. 10** Cyclic voltammogram of catalyst Ia in 0.1 M HClO₄ + 0.5 M CH₃OH at room temperature**Fig. 11** Cyclic voltammogram of Cat Ia (straight line), IIa (dashed line), and IIIa (dotted line) in 0.1 M HClO₄ + 0.5 M CH₃OH at room temperature

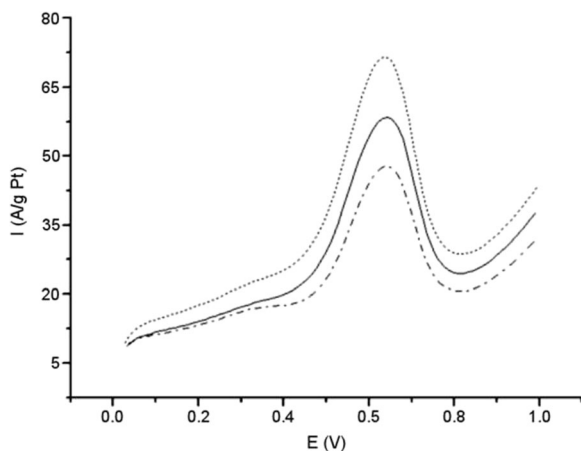


Fig. 12 Cyclic voltammogram of Cat Ib (straight line), IIb (dashed line), and IIIb (dotted line) in 0.1 M HClO₄ + 0.5 M CH₃OH at room temperature

constant and the surfactants were changed (Figs. 14, 15, and 16), it was found out that the most active catalyst was Cat c which was prepared by N,N-dimethyl-1-heptanamine and the least active was Cat b which was synthesized by N-methyl-1-heptanamine. The highest performance was obtained by Cat IIIc, ~ 167 A/g Pt, in which the performance of the catalyst is increased by 2.23 times compared to commercially available ETEK 40wt%Pt/Vulcan XC72 catalysts (Kim and Mitani 2006) as shown in Figs. 13 and 16; indicating that both surfactant and reducing agent have a significant effect on the performance of the catalysts. In addition to this, the I_p/I_r ratio was also determined for all catalysts (Table 6), and found that

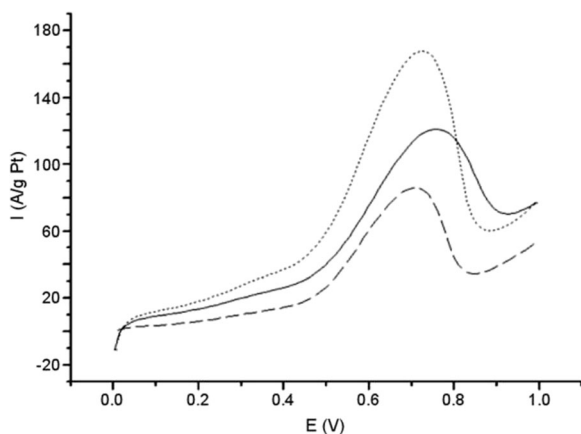


Fig. 13 Cyclic voltammogram of Cat Ic (straight line), IIc (dashed line), and IIIc (dotted line) in 0.1 M HClO₄ + 0.5 M CH₃OH at room temperature

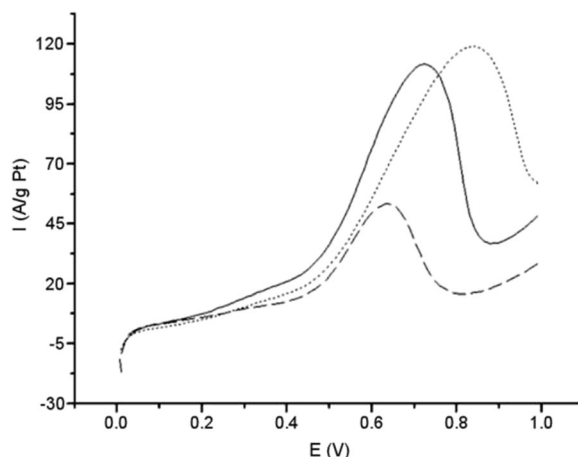


Fig. 14 Cyclic voltammogram of Cat Ia (straight line), Ib (dashed line), and Ic (dotted line) in 0.1 M HClO₄ + 0.5 M CH₃OH at room temperature

it was the highest for Cat IIIc, showing that this catalyst has the smallest amount of poison formation on the surface of catalyst.

In order to try and understand the reasons behind the performance of catalysts, chemical surface area (CSA), electrochemical surface area (ESCA), percent platinum utility (% Pt utility), and roughness factor (RF) of each catalyst were calculated. For this purpose, the CSA of the platinum was determined using following formula (Li et al. 2004):

$$\text{CSA (m}^2/\text{g Pt)} = 6000/(\rho \cdot d)$$

where ρ is average density of Pt metal (21.4 g/cm³) and d is the mean diameter of Pt particles in nm which was

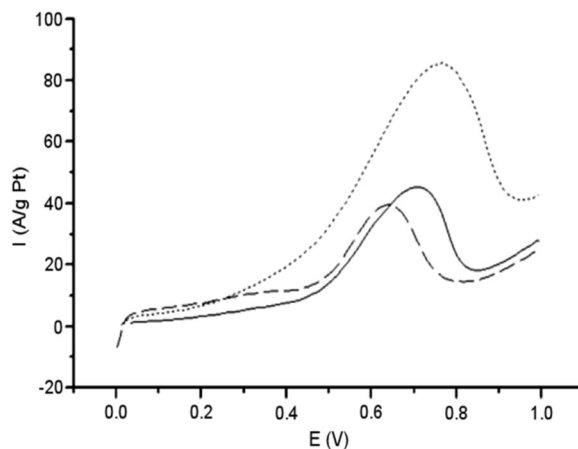


Fig. 15 Cyclic voltammogram of Cat IIa (straight line), IIb (dashed line), and IIc (dotted line) in 0.1 M HClO₄ + 0.5 M CH₃OH at room temperature

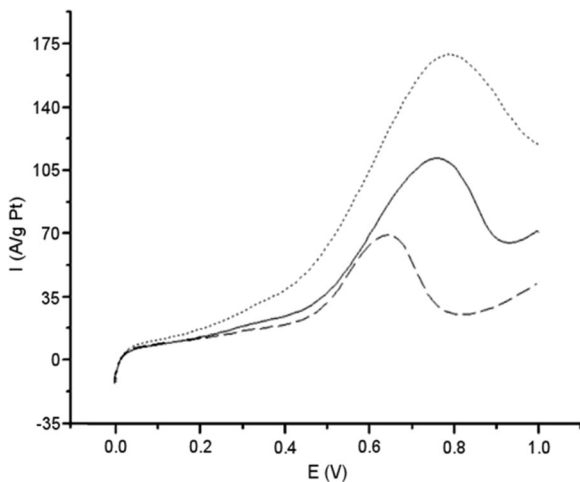


Fig. 16 Cyclic voltammogram of Cat IIIa (straight line), IIIb (dashed line), and IIIc (dotted line) in 0.1 M HClO₄ + 0.5 M CH₃OH at room temperature

calculated from XRD and TEM data. The results are given in Table 6. As can be seen from the table, there is only a small difference between the CSA values of the catalysts, due to similar particle sizes. The highest CSA value was obtained for Cat III, ~64 m²/g Pt and the lowest value was observed for Cat I, ~49 m²/g Pt. The electrochemical surface area (ECSA) of the catalysts was calculated using the cyclic voltammograms and ICP results. The formula is given below (Lee et al. 1998):

$$ECSA \text{ (cm}^2\text{/g Pt)} = Q/(a \cdot b)$$

where *Q* = charge (mC/cm² Pt) calculated from hydrogen desorption region, *a* = constant, 0.21 mC/cm² Pt,

and *b* = amount of platinum in g/cm² electrode. The average ECSA was found to be ~33.36, 23.21, and 49.38 cm²/g Pt for Cat I, II, and III, respectively (Table 6); showing that the type of reducing affects ESCA more than surfactant type. CSA and ECSA data were used to calculate percent platinum utility (Table 6), using the following formula:

$$\%Pt \text{ Utility} = ECSA \cdot 100 / CSA$$

The order of percent platinum utility is Cat II < Cat I < Cat III and the highest value was obtained for Cat IIIc. Besides CSA and ECSA, roughness factor (RF) was also calculated by using the following formula (Mayrhofer et al. 2008):

$$RF = \text{Real area} / \text{Geometrical area}$$

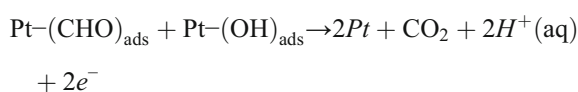
Real area = *Q*_{hyd} (mC)/0.21 mC/cm², where *Q*_{hyd} is the charge calculated from hydrogen desorption region, geometrical area, π*r*² = 0.38 cm², where *r* is the radius of electrode, 0.35 cm. The RF results showed the same trend as the ECSA values (Table 6).

In summary, FTIR and DFT studies indicated that surfactants used in the syntheses decompose to form partially crystalline carbon and chemical and electrochemical studies indicated that the kind of surfactants and reducing agents are important parameters on the performance of the catalysts. Within each group (Cat I, II, and III), the order of electrochemical surface area and performance of the catalysts is Cat b < Cat a < Cat c, it does not matter which reducing agent is used. This sequence is as expected because there is a direct correlation between performance and

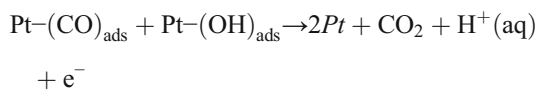
Table 6 CSA and percent platinum utility found from TEM and XRD data, ECSA, roughness factor (RF), and I_f/I_r for all catalysts

Catalysts	CSA (m ² /gPt) (TEM)	CSA (m ² /gPt) (XRD)	a- b	ECSA (m ² /g Pt)	% Pt utility (TEM)	% Pt utility (XRD)	c- d	RF	I _f /I _r
Cat Ia	46.73	45.22	1.51	32.58	69.73	72.04	2.31	50.02	1.11
Cat Ib	50.07	47.52	2.55	31.74	63.40	66.79	3.39	49.01	1.08
Cat Ic	50.98	51.92	0.94	35.77	70.17	68.89	1.28	54.20	1.19
Cat IIa	52.90	56.07	3.17	21.53	40.70	38.40	2.30	32.62	1.15
Cat IIb	52.90	52.90	0.00	20.20	38.19	38.18	0.01	32.01	1.01
Cat IIc	66.76	62.31	4.45	27.90	41.80	44.78	2.98	42.32	1.20
Cat IIIa	62.30	58.41	3.89	48.67	78.13	83.32	5.19	73.74	1.12
Cat IIIb	66.76	68.38	1.62	47.07	70.51	68.84	1.67	72.30	1.09
Cat IIIc	63.72	62.31	1.41	52.39	82.22	84.08	1.86	78.01	1.68

electrochemical surface area of catalysts. As the surfactant is kept constant, H_2O_{ads} , average surface area (BET) and performance of the catalysts increase from Cat II to Cat I to Cat III. The average surface area and performance relation is obvious, and H_2O_{ads} and performance can be explained by the proposed mechanism which is derived from previous in-situ experimental techniques. According to the proposed mechanism the adsorption of H_2O is need to form the product of the methanol oxidation reaction. In this context, H_2O_{ads} converts to OH_{ads} and reacts with CHO_{ads} to form CO_2 as given below (Yang et al. 2007; Beden et al. 1992).



On the other hand, surface coverage by poison (CO) is the largest for Cat II and smallest for Cat III. It is well known that the surface poisoning delays the methanol oxidation reaction, however CO_{ads} is oxidized to CO_2 by OH_{ads} at more positive potentials (Léger 2001).



Conclusion

In this study, carbon-supported platinum nanoparticles were prepared using different surfactants and reducing agents. It was found that surfactants decompose to form partially crystalline carbon and platinum crystallizes in face-centered cubic (fcc) structure for all catalysts and they are in the form of small and agglomerated particles with different shapes, sizes, and densities, depending on kind of surfactants and reducing agents used. Cat IIIc displayed the highest performance towards methanol oxidation reaction, because it has highest electrochemical surface area, percent platinum utility, roughness factor, and I_p/I_r ratio.

Acknowledgements We gratefully acknowledge Türkiye Bilimsel ve Teknolojik Araştırma Kurumu (TÜBİTAK-111T162) for financial support. We also thank Dr. Michael Pitcher for proof-reading this manuscript, Gerçem Altunordu for FTIR measurements, and Toprak Seda Karaosmanoğlu for the computer work.

We also thank TÜBİTAK ULAKBİM, High Performance and Grid Computing Center (TR-Grid e-Infrastructure) for the calculations reported in the theoretical part of this paper.

Funding This study was funded by Türkiye Bilimsel ve Teknolojik Araştırma Kurumu (TÜBİTAK-111T162).

Compliance with ethical standards

Conflict of interest The authors declare that they have no conflict of interest.

References

- Ahmed MS, Kim D, Jeon S (2013) Covalently grafted platinum nanoparticles to multi walled carbon nanotubes for enhanced electrocatalytic oxygen reduction. *Electrochim Acta* 92:168–175. <https://doi.org/10.1016/j.electacta.2012.10.160>
- Arico AS, Srinivasan S, Antonucci V (2001) DMFCs: from fundamental aspects to technology development. *Fuel Cells* 1(2):133–161. [https://doi.org/10.1002/1615-6854\(200107\)1:2<133::AID-FUCE133>3.0.CO;2-5](https://doi.org/10.1002/1615-6854(200107)1:2<133::AID-FUCE133>3.0.CO;2-5)
- Asif M, Muneer T (2007) Energy supply, its demand and security issues for developed and emerging economies. *Renew Sust Energ Rev* 11(7):1388–1413. <https://doi.org/10.1016/j.rser.2005.12.004>
- Bagotsky V S (2012) Fuel cells: problems and solutions, vol 56. John Wiley & Sons, Inc., Hoboken, New Jersey
- Barone V, Cossi M (1998) Quantum calculation of molecular energies and energy gradients in solution by a conductor solvent model. *J Phys Chem A* 102(11):1995–2001. <https://doi.org/10.1021/jp9716997>
- Beden B, Leger J M, Lamy C (1992) Modern aspects of electrochemistry, Kluwer Academic/Plenum Publishers, 22, 97, New York
- Carette L, Friedrich KA, Stimming U (2000) Fuel cells: principles, types, fuels, and applications. *ChemPhysChem* 1(4):162–193. [https://doi.org/10.1002/1439-7641\(20001215\)1:4<162::AID-CPHC162>3.0.CO;2-Z](https://doi.org/10.1002/1439-7641(20001215)1:4<162::AID-CPHC162>3.0.CO;2-Z)
- Carette L, Friedrich KA, Stimming U (2001) Fuel cells—fundamentals and applications. *Fuel Cells* 1(1):5–39. [https://doi.org/10.1002/1615-6854\(200105\)1:1<5::AID-FUCE5>3.0.CO;2-G](https://doi.org/10.1002/1615-6854(200105)1:1<5::AID-FUCE5>3.0.CO;2-G)
- Casella IG, Guascito MR, Sannazzaro MG (1999) Voltammetric and XPS investigations of nickel hydroxide electrochemically dispersed on gold surface electrodes. *J Electroanal Chem* 462(2):202–210. [https://doi.org/10.1016/S0022-0728\(98\)00413-6](https://doi.org/10.1016/S0022-0728(98)00413-6)
- Chatterjee SK (2010) X-ray diffraction: its theory and applications, PHI learning Pvt. Ltd., New Delhi
- Frisch MJ, Trucks GW, Schlegel HB, Scuseria GE, Robb MA, Cheeseman JR, Nakatsuji H (2009) Gaussian 09 revision A. 02-SMP. Gaussian Inc., Wallingford
- Gökagaç G, Kennedy BJ, Cashion JD, Brown LJ (1993) Characterisation of carbon-supported Pt–Sn bimetallic catalysts for the electrochemical oxidation of methanol. *J Chem*

- Soc Faraday Trans 89(1):151–157. <https://doi.org/10.1039/FT9938900151>
- Hart AB, Womack GJ (1967) Fuel cells: theory and application. Chapman & Hall, London
- Hogarth MP, Hards GA (1996) Direct methanol fuel cells. *Platin Met Rev* 40(4):150–159
- Hordeski MF (2009) Hydrogen & fuel cells: advances in transportation and power. The Fairmont Press, Inc., New York
- Huang Y, Zhai Z, Luo Z, Liu Y, Liang Z, Fang Y (2014) A facile one-pot self-assembly approach to incorporate SnO_x nanoparticles in ordered mesoporous carbon with soft templating for fuel cells. *Nanotechnology* 25(13):135403. <https://doi.org/10.1088/0957-4484/25/13/135403>
- Huang ZD, Zhang B, Oh SW, Zheng QB, Lin XY, Yousefi N, Kim JK (2012) Self-assembled reduced graphene oxide/carbon nanotube thin films as electrodes for supercapacitors. *J Mater Chem* 22(8):3591–3599. <https://doi.org/10.1039/C2JM15048D>
- Kim YT, Mitani T (2006) Surface thiolation of carbon nanotubes as supports: a promising route for the high dispersion of Pt nanoparticles for electrocatalysts. *J Catal* 238:394–401. <https://doi.org/10.1016/j.jcat.2005.12.020>
- Kulkarni A, Ciacchi FT, Giddey S, Munnings C, Badwal SPS, Kimpton JA, Fini D (2012) Mixed ionic electronic conducting perovskite anode for direct carbon fuel cells. *Int J of Hydrogen Energy* 37(24):19092–19102. <https://doi.org/10.1016/j.ijhydene.2012.09.141>
- Kvande I, Zhu J, Zhao TJ, Hammer N, Rønning M, Raaen S, Chen D (2010) Importance of oxygen-free edge and defect sites for the immobilization of colloidal Pt oxide particles with implications for the preparation of CNF-supported catalysts. *J Phys Chem C* 114(4):1752–1762. <https://doi.org/10.1021/jp906572z>
- Lee SJ, Mukerjee S, McBreen J, Rho YW, Kho YT, Lee TH (1998) Effects of Nafion impregnation on performances of PEMFC electrodes. *Electrochim Acta* 43(24):3693–3701. [https://doi.org/10.1016/S0013-4686\(98\)00127-3](https://doi.org/10.1016/S0013-4686(98)00127-3)
- Léger JM (2001) Mechanistic aspects of methanol oxidation on platinum-based electrocatalysts. *J Appl Electrochem* 31(7):767–771. <https://doi.org/10.1023/A:1017531225171>
- Li X (2006) Principles of fuel cells. Taylor&Francis Group, New York
- Li W, Zhou W, Li H, Zhou Z, Zhou B, Sun G, Xin Q (2004) Nanostructured Pt–Fe/C as cathode catalyst in direct methanol fuel cell. *Electrochim Acta* 49(7):1045–1055. <https://doi.org/10.1016/j.electacta.2003.10.015>
- Liang L, Sun G, Sun S, Liu J, Tang S, Li H, Zhou B, Xin Q (2005) Structure and chemical composition of supported Pt–Sn electrocatalysts for ethanol oxidation. *Electrochim Acta* 50:5384–5389. <https://doi.org/10.1016/j.electacta.2005.03.018>
- Luo PF, Kuwana T, Paul DK, Sherwood PM (1996) Electrochemical and XPS study of the nickel–titanium electrode surface. *Anal Chem* 68(19):3330–3337. <https://doi.org/10.1021/ac960236e>
- Mayrhofer KJJ, Strmcnik D, Bliznac BB, Stamenkovic V, Arenz M, Markovic NM (2008) Measurement of oxygen reduction activities via the rotating disc electrode method: from Pt model surfaces to carbon-supported high surface area catalysts. *Electrochim Acta* 53(7):3181–3188. <https://doi.org/10.1016/j.electacta.2007.11.057>
- Senthilnathan J, Liu YF, Rao KS, Yoshimura M (2014) Submerged liquid plasma for the synchronized reduction and functionalization of graphene oxide. *Sci Rep* 4:4395. <https://doi.org/10.1038/srep04395>
- Singh S, Datta J (2010) Size control of Pt nanoparticles with stabilizing agent for better utilization of the catalyst in fuel cell reaction. *J Mater Sci* 45(11):3030–3040. <https://doi.org/10.1007/s10853-010-4307-9>
- Stambouli AB, Traversa E (2002) Solid oxide fuel cells (SOFCs): a review of an environmentally clean and efficient source of energy. *Renew Sust Energy Rev* 6(5):433–455
- Şen F, Gökağaç G, Şen S (2013) High performance Pt nanoparticles prepared by new surfactants for C1 to C3 alcohol oxidation reactions. *J Nanopart Res* 15(10):1979. <https://doi.org/10.1007/s11051-013-1979-5>
- Şen F, Gökağaç G (2014) Pt nanoparticles synthesized with new surfactants: improvement in C1–C3 alcohol oxidation catalytic activity. *J Appl Electrochem* 44(1):199–207. <https://doi.org/10.1007/s10800-013-0631-5>
- Şen F, Şen S, Gökağaç G (2011) Efficiency enhancement of methanol/ethanol oxidation reactions on Pt nanoparticles prepared using a new surfactant, 1, 1-dimethyl heptanethiol. *Phys Chem Chem Phys* 13(4):1676–1684. <https://doi.org/10.1039/C0CP01212B>
- Şen F, Gökağaç G (2007) Different sized platinum nanoparticles supported on carbon: an XPS study on these methanol oxidation catalysts. *J Phys Chem C* 111(15):5715–5720. <https://doi.org/10.1021/jp068381b>
- Rao KS, Senthilnathan J, Liu YF, Yoshimura M (2014) Role of peroxide ions in formation of graphene nanosheets by electrochemical exfoliation of graphite. *Sci Rep* 4(4237):1–17. <https://doi.org/10.1038/srep04237>
- Tien HW, Huang YL, Yang SY, Hsiao ST, Liao WH, Li HM, Wang YS, Wang JY, Ma CCM (2012) Preparation of transparent, conductive films by graphene nanosheet deposition on hydrophilic or hydrophobic surfaces through control of the pH value. *J Materials Chemistry* 22:2545–2552. <https://doi.org/10.1039/C1JM14564A>
- Tomasi J, Mennucci B, Cammi R (2005) Quantum mechanical continuum solvation models. *Chem Rev* 105(8):2999–3094. <https://doi.org/10.1021/cr9904009>
- Wang Y, Li L, Hu L, Zhuang L, Lu J, Xu B (2003) A feasibility analysis for alkaline membrane direct methanol fuel cell: thermodynamic disadvantages versus kinetic advantages. *Electrochem Commun* 5(8):662–666. [https://doi.org/10.1016/S1388-2481\(03\)00148-6](https://doi.org/10.1016/S1388-2481(03)00148-6)
- Wasmus S, Küver A (1999) Methanol oxidation and direct methanol fuel cells: a selective review. *J Electroanal Chem* 461(1):14–31. [https://doi.org/10.1016/S0022-0728\(98\)00197-1](https://doi.org/10.1016/S0022-0728(98)00197-1)
- Wu Z, Huang XL, Wang ZL, Xu JJ, Wang HG, Zhang XB (2014) Electrostatic induced stretch growth of homogeneous β-Ni(OH) 2 on graphene with enhanced high-rate cycling for supercapacitors. *Sci Rep* 4:3669. <https://doi.org/10.1038/srep03669>
- Yang GW, Gao GY, Zhao GY, Li HL (2007) Effective adhesion of Pt nanoparticles on thiolated multi-walled carbon nanotubes and their use for fabricating electrocatalysts. *Carbon* 45(15):3036–3041. <https://doi.org/10.1016/j.carbon.2007.06.021>
- Yang J, Deivaraj TC, Too HP, Lee JY (2004a) An alternative phase-transfer method of preparing alkylamine-stabilized

- platinum nanoparticles. *J Phys Chem B* 108(7):2181–2185. <https://doi.org/10.1021/jp036190s>
- Yang J, Lee JY, Deivaraj TC, Too HP (2004b) An improved Brust's procedure for preparing alkylamine stabilized Pt, Ru nanoparticles. *Colloids Surf A Physicochem Eng Asp* 240(1):131–134. <https://doi.org/10.1016/j.colsurfa.2004.03.019>
- Yang SY, Chang KH, Tien HW, Lee YF, Li SM, Wang YS, Hu CC (2011) Design and tailoring of a hierarchical graphene-carbon nanotube architecture for supercapacitors. *J Mater Chem* 21(7):2374–2380. <https://doi.org/10.1039/C0JM03199B>
- Zeng J, Yang J, Lee JY, Zhou W (2006) Preparation of carbon-supported core-shell Au–Pt nanoparticles for methanol oxidation reaction: the promotional effect of the Au core. *J Phys Chem B* 110(48):24606–24611. <https://doi.org/10.1021/jp0640979>
- Zheng W (2012) A novel structure of a direct methanol fuel cell, doctor of philosophy thesis in chemistry. University of Turku, Salo